Available online at www.sciencedirect.com

SciVerse ScienceDirect

Energy Procedia 34 (2013) 407 – 416

Energy Procedia

10th Eco-Energy and Materials Science and Engineering (EMSES2012)

Unsteady Surface Pressures and Airload of a Pitching Airfoil

Supakit Worasinchai[a,*], Grant Ingram[b], and Robert Dominy[b]

[a]*National Metal and Materials Technology Center (MTEC), 114 Paholyothin Road, Klong Luang, Pathumthani, Thailand, 12120*
[b]*School of Engineering and Computing Sciences, Durham University, South Road, Durham DH1 3LE*

Abstract

This paper presents unsteady surface pressure variations of a symmetrical NACA0012 section commonly used on Vertical-axis wind turbine blades. The section was tested at a Reynolds number of 90,000, mean incidence angles of 15° and -15°, and a reduced frequency of 0.20. The experimental results show that the airfoil motion had significant effects on surface pressure distribution over the airfoil, leading to a formation and shedding of an energetic leading edge vortex which strongly affects the overall airload over the incidence range.

Selection and peer-review under responsibility of COE of Sustainalble Energy System, Rajamangala University of Technology Thanyaburi (RMUTT)

Keywords: Airfoil; Dynamic performance characteristics; Low Reynolds number; Vortex formation.

1. Introduction

The concern about global warming has initiated a renewed interest in renewable energy sources. Wind energy is one of the sources that play a significant role in electricity production and the use of wind turbines to supply electricity has grown very rapidly in the last decade [1]. The Thai government itself has issued a renewable policy and has set a plan to increase wind power capacity to be 800MW in 2022 [2]. Current installation is now at 5.13MW [2]. Different types of wind turbines (horizontal- and vertical-axis) with different sizes (large- and small-scale) can be implemented in parallel to meet the target set.

The Darrieus-type (vertical-axis) wind turbine (Fig.1) is attractive in terms of simple blade design and manufacture. It is also better suited to the urban environment where wind direction rapidly changes as it is insensitive to wind direction. However, the turbine is commonly believed to be non self-starting [4], [5].

* Corresponding author.
E-mail address: supakitw@mtec.or.th .

Selection and peer-review under responsibility of COE of Sustainalble Energy System, Rajamangala University of Technology Thanyaburi (RMUTT)
doi:10.1016/j.egypro.2013.06.769

Nomenclature

α	Incidence angle
C_N	Normal force coefficient
C_P	Pressure coefficient
k	Reduced frequency
Re	Reynolds number

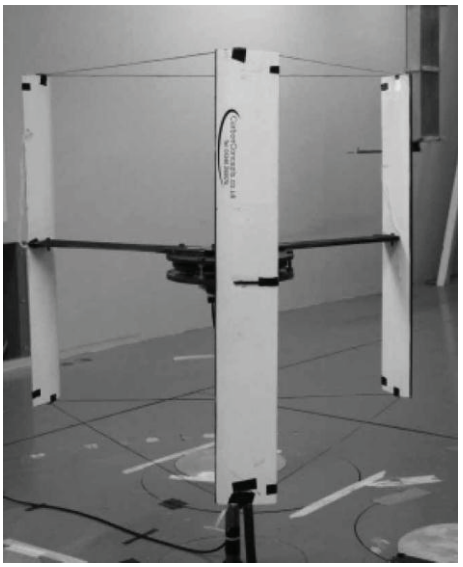

Fig. 1. An example of a Darrieus rotor [3]

Despite this perception, it has been increasingly reported that the turbine can self-start in even its simplest configuration of fixed-pitch, straight blades with a symmetrical airfoil section [3], [6], and [7]. A recent investigation based upon the analogy between the airfoil in Darrieus motion and flapping-wing flow mechanism has revealed that the airfoil in Darrieus motion is associated with propulsion mechanism as that is found in flapping-wing system [8], suggesting that the unsteadiness associated with the rotor is key to resolve the inconsistent findings. It also suggests that the flow over blade rotation can be modeled by a flapping motion and airfoil dynamic performance obtained from simple pitching motion can be roughly used to investigate the effects of unsteadiness [9].

Experimental investigations of airfoils in pitch motion is of interest and had been studied at very high Reynolds numbers as it was intended for aircraft [10] and helicopter applications [11]. This unsteady data however cannot be directly applied to the Darrieus rotor analysis as the flow conditions are significantly different.

One of the most relevant information is the experiments tested by Gerotakos [12]. In his tests, a NACA0012 section was tested at a Reynolds number of 135,000 and a reduced frequency of 0.099. Although this information is useful, it is not sufficient to show how the unsteadiness will actually affect the Darrieus rotor performance, particularly at a lower Reynolds number and a higher reduced frequency.

This paper further investigates such effects and provides additional performance characteristics at flow conditions that the Darrieus blades typically experience.

2. Wind tunnel configuration

The wind tunnel used for the investigation was the 0.5m Plint wind tunnel at Durham University (Fig. 2). The wind tunnel testing section was configured to have a square cross-section of 457mm x 457mm with solid sides but open top and bottom to avoid wall proximity effects [9]. The airfoil motion considered here is a harmonically sinusoidal motion. The motion was generated by the use of crank mechanism which is powered by a 250W DC motor (Fig. 2).

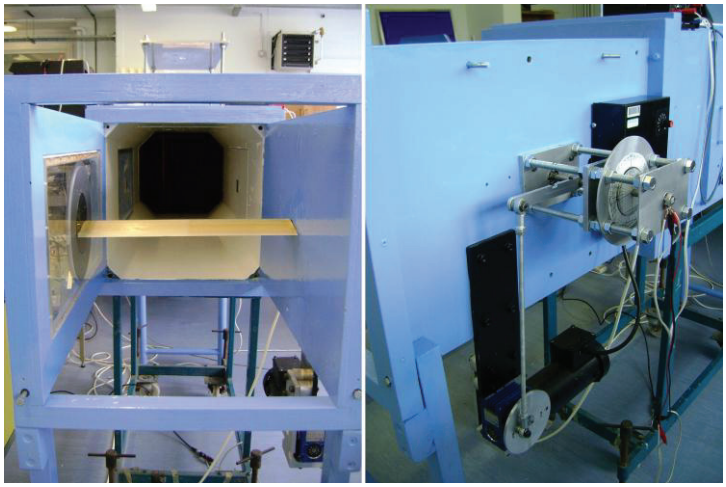

Fig. 2. Wind tunnel and oscillating system

To suit the test section, the airfoil was designed to have a span of 0.450 m and a chord of 0.11m resulting in both section H/C ratio and the airfoil aspect ratio having a value of 4.1. Initial CFD evaluation confirmed that this test configuration resulted in 2D flow over much of the airfoil's span whilst retaining a large enough cross section to contain the required internal instrumentation [9]. The airfoil was produced by rapid prototyping from Fullcure 720 material, giving a high surface precision (±0.1mm).

Pressure tappings were located at midspan to measure the nominally two dimensional pressure coefficient. The number of pressure tappings was 28 and the pitching axis was located at quarter chord. All tappings were connected to a 48-channel Scanivalve which was connected to a pressure transducer and a data logger.

A computer-based system was used to record all signals via an NI USB-6218 ADC consisting of 16 channels with a resolution of 16 bits. This device has a sample rate of up to 250 kS/s. In addition to the steady-state calibration of the pressure transducers, the system dynamic response was performed to account the damping effect of the system. This response is taken into consideration using transfer function correction [13]. Repeatability of the measurements was good with standard deviation of ±0.16. More detail of the experiments can be found in [9].

3. Experimental results

The dynamic performance characteristics of the airfoil are discussed in terms of unsteady chordwise pressure distributions and unsteady normal force. Discussion of the C_P distributions over a series of incidence ranges will be first presented to show how unsteady flow phenomena such as vortex formation and shedding affect the pressure variations. The overall effect of these flows on aerodynamic loadings is illustrated in the form of unsteady C_N (obtained by integrating the unsteady surface pressure over the airfoil chord) over the incidence range.

Since each motion is associated with different flow phenomena, the presentation of unsteady surface pressure distributions are divided into four cases (Fig. 3).

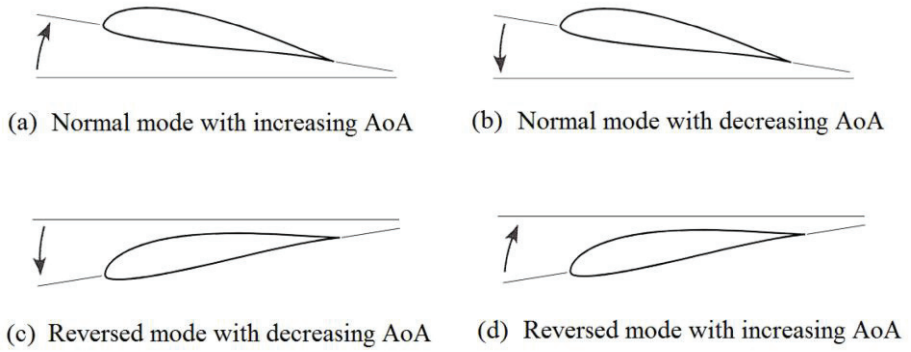

Fig. 3. Normal and reversed modes of operation

(1) *Normal mode with increasing incidence angle* - The incidence angle is positive and increasing in this motion. Flow characteristics associated with this motion are vortex formation and convection which can be observed by higher-than-normal suction peak at the leading edge and a wave-like pressure variation along the airfoil chord, respectively.

(2) *Normal mode with decreasing incidence angle* - In this motion, the incidence range is still positive but decreasing (pitch-down motion). The primary flow feature associated with this motion is flow reattachment. The reattachment typically occurs at the leading edge and can be observed from the C_P variation that begins to follow the airfoil nose shape.

(3) *Reversed cambered mode with decreasing incidence angle* - In this mode, the incidence is negative and decreasing. This motion is mirrored of the first mode and the formation and convection of dynamic-stall vortex take place on the pressure side.

(4) *Reversed cambered mode with increasing incidence angle* - The incidence angle increases back to the neutral position in this motion. The flow will reattach and regain its suction peak as the airfoil returns to the normal mode.

3.1. Unsteady pressure variations

Figure 4 presents unsteady surface pressure coefficients for the NACA0012 at ascending incidence angles of 10° to 20° with a 2° increment at a reduced frequency of 0.20 (4a to 4f). As noted before, this incidence change is associated with a vortex formation process.

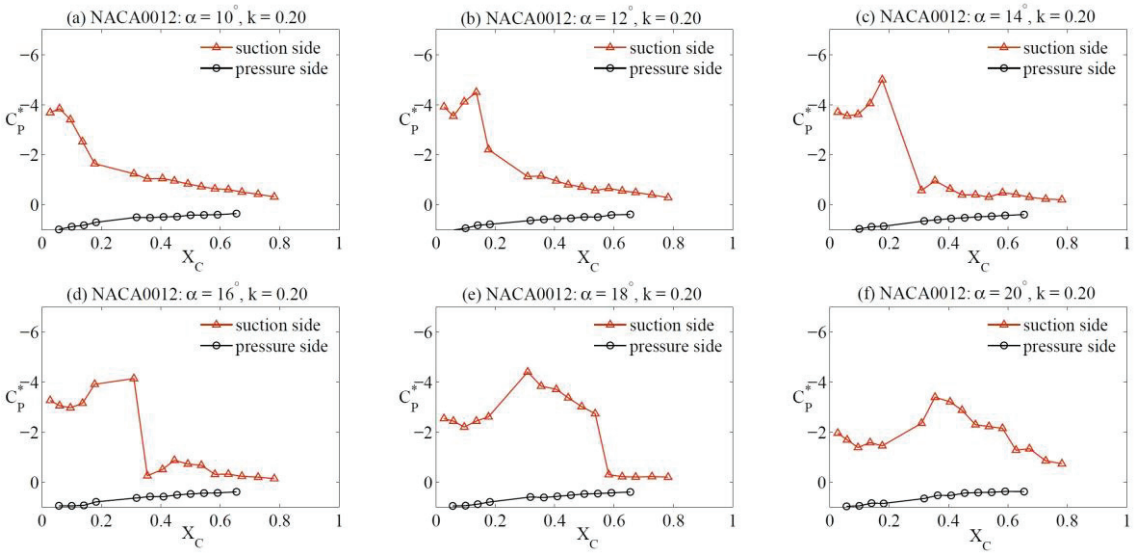

Fig. 4. Unsteady C_P at a reduced frequency of 0.2: normal mode with pitch-up motion

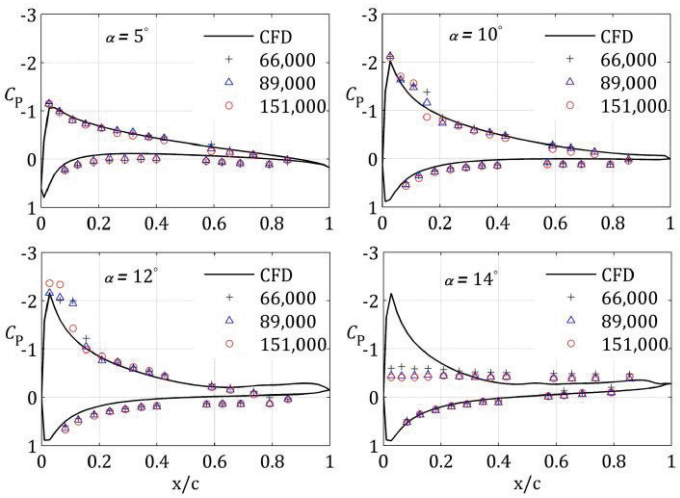

Fig. 5. Steady C_P of a NACA0012 section

It can be observed that the C_Ps are fundamentally different from those was found statically where the suction peak is always around the leading edge of the airfoil (Fig. 4 and 5). Under dynamic conditions,

the peak pressure (or dynamic-stall vortex) is strong (around -4, double of that was found statically) and will transverse along the airfoil chord, causing a wave-like C_P curves.

The higher strength of suction peak results in a low rate of convection and the stall is postponed to a higher incidence angle. The state of full stall occurs at 24° at the reduced frequency of 0.20.

In this normal mode where the incidence decreases (pitch-down motion), the flow is typically separated and will try to reattach from the leading edge when the incidence angle is sufficiently low. Figure 6 shows unsteady C_Ps at selected incidences of 30°, 28°, 26°, 20°, 10°, and 5° (6a to 6f). It can be seen that the flow separation (as indicated by the flat C_P curve) persists until the incidence angle is around 10°. This delay in flow reattachment, together with the delay of stall during the pitch-up motion, causing a hysteresis in dynamic loads over the incidence range (will be presented later).

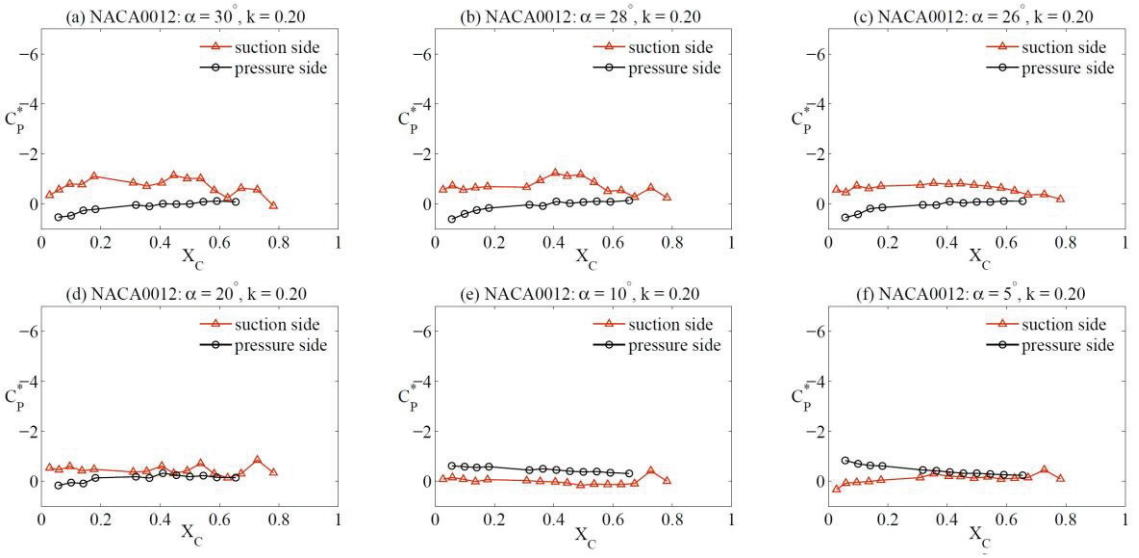

Fig. 6. Unsteady C_P at a reduced frequency of 0.2: normal mode with pitch-down motion

In the reversed camber operation, the suction and pressure sides are reversed (Fig. 7). The suction peak and formation of dynamic-stall vortex will take place on the pressure side (solid line with circles).

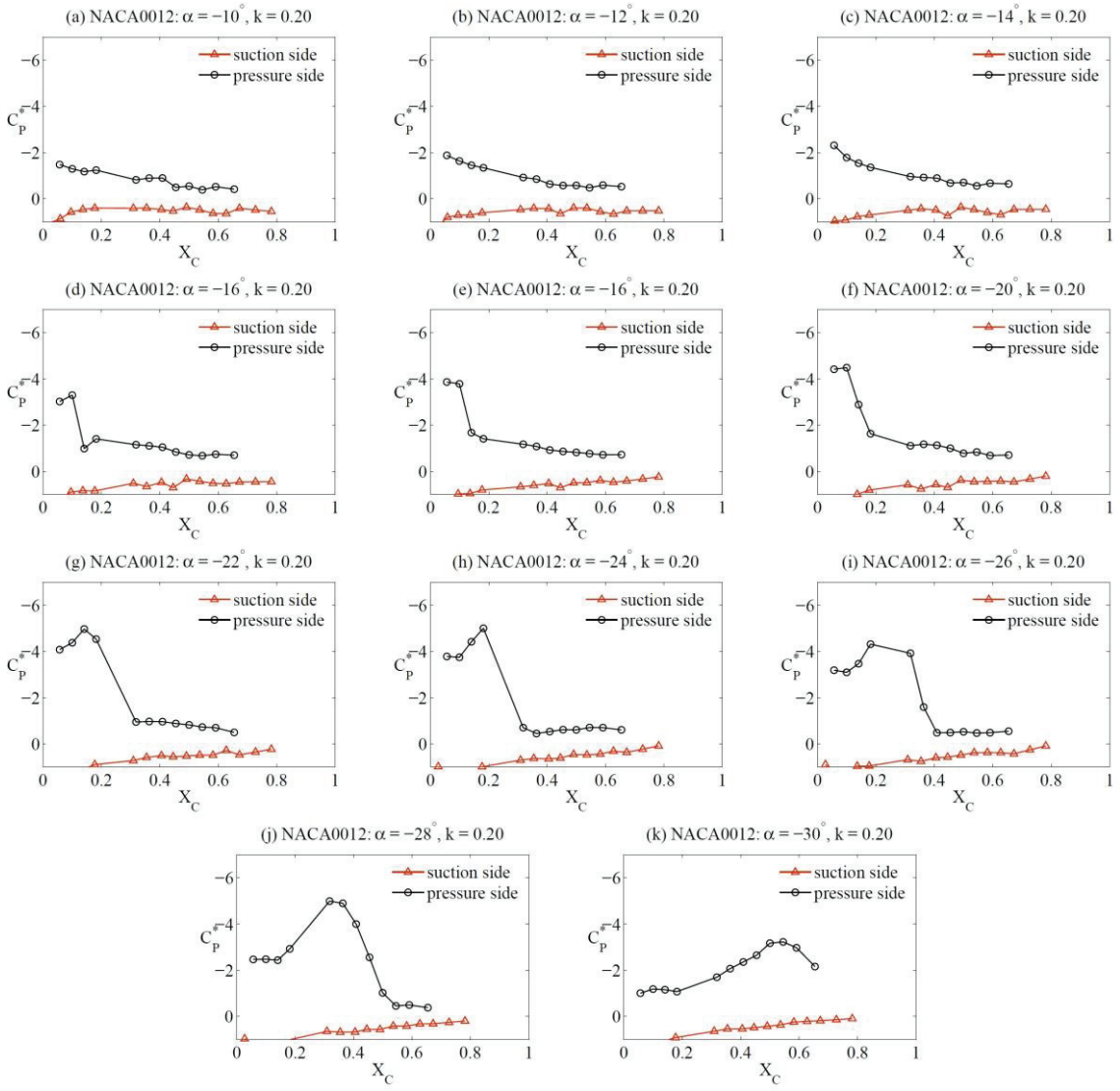

Fig. 7. Unsteady C_P at a reduced frequency of 0.2: reversed mode with pitch-down motion

It is observed that the maximum suction peak is approximate -5 at a reduced frequency of 0.20 and the vortex convects along the airfoil at a significantly slow rate (Fig. 7f to 7k), causing the full stall to occur at -30°. This slower rate of convection suggests that the vortex experiences flow conditions that are different from that of the normal mode.

The difference between these two modes is thought to be a result of the incoming flow. In the normal mode, the vortex seems to be more diffuse and can be swept away by the incoming flow (Fig. 8). In the reversed cambered mode the vortex is not significantly affected by the flow and the vortex strength is nearly constant when travelling along the airfoil chord. Moreover, the incoming flow over the trailing

edge seems to force the vortex to convect at a slower rate, resulting in imbalance flow behavior on this symmetrical section.

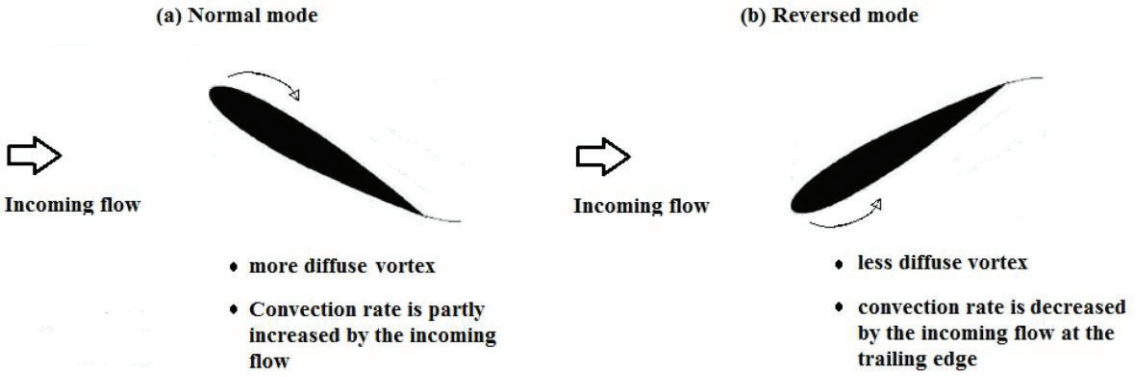

Fig. 8. Flow schematics of normal and reversed camber modes of operation

During pitch-up motion of the reversed camber mode, the flow recovers and the suction and pressure sides will return to their normal mode of operation (Fig. 9). The flow on the pressure side, as expected, is fully stalled at the beginning of the pitch-up motion. The pressure regains its peak with increasing incidence angle.

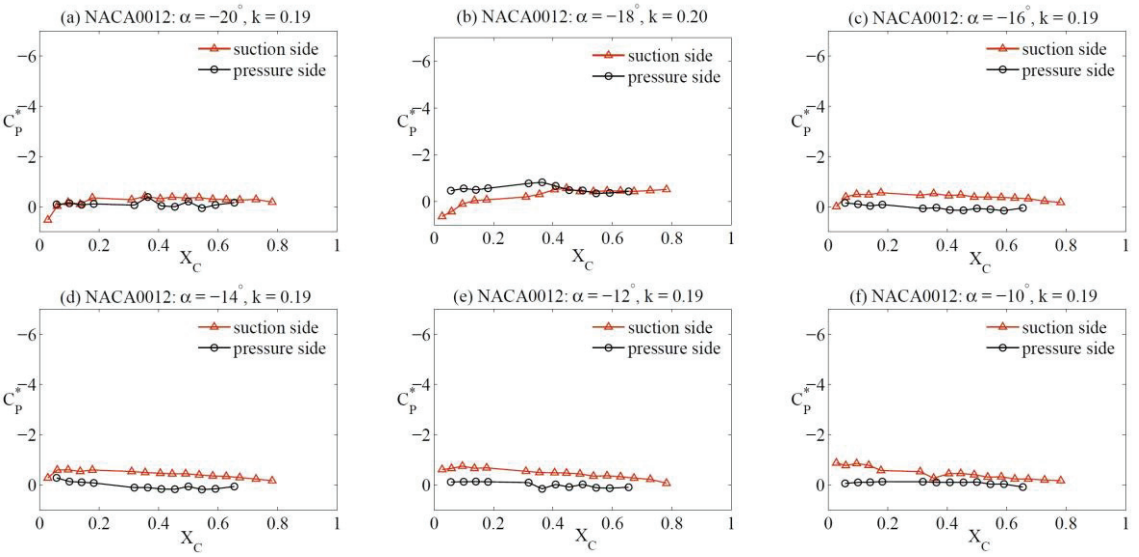

Fig. 9. Unsteady C_P at a reduced frequency of 0.2: reversed mode with pitch-up motion

3.2. Unsteady airload

The transient behavior in the four different modes leads to a hysteresis in aerodynamic airload. Figure 10 presents a variation of unsteady normal force coefficient together with its static counterpart (dotted line).

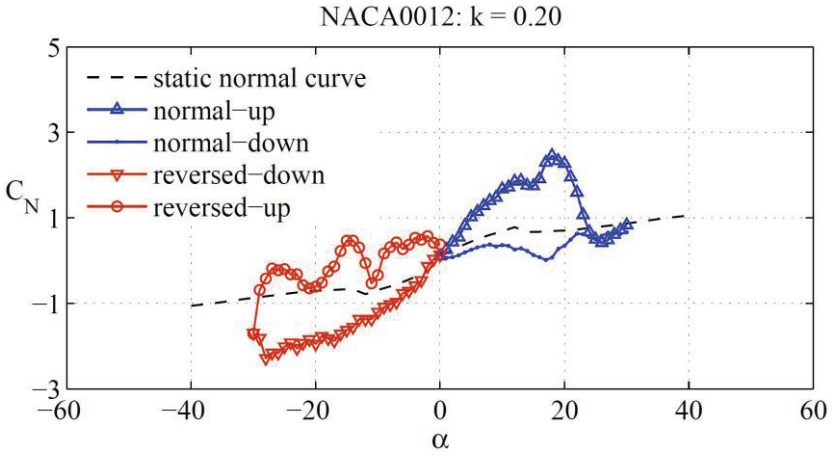

Fig. 10. Unsteady airload

It is apparent that, in the normal mode, dynamic-stall formation generated by the airfoil motion overshoots the C_N to around 2 (solid line with triangles). After the vortex shedding, the C_N drops to around its static value which continuously decreases during pitch-down motion (solid line with points).

In reversed camber operation, the imbalance flow feature promotes an overshoot of the C_N to around -2.5 at an incidence angle of 30°.

4. Conclusion

Unsteady surface pressure variations of the NACA0012 airfoil at a low Reynolds number and a high reduced frequency had been investigated in this paper. The results indicate that the unsteadiness caused by the airfoil motion is significant and related to the formation of energetic leading edge vortex. This phenomenon leads to an increase in airload and delay of stall which implies that the energetic leading edge vortex can be exploited to generate an additional force. The existence of this force can be used to promote the turbine ability to start and to enhance the rotor performance.

Acknowledgement

The assistance of Collin Wintrip, Roger Little, Anthony Collinson, Phillip Duff, and Ian Garrrett in setting up the experiment is gratefully acknowledged.

References

[1] Global Wind Energy Council. Global Wind Power Boom Continues Despite Economic Woes, Retrieved June 04, 2012 from the World Wide Web: http://www.gwec.net

[2] Department of Alternative Energy Development and Efficiency. Energy in Thailand: Facts & Figures, Retrieved October 04, 2012 from the World WideWeb: http://www.dede.gp.th

[3] Hill N, Dominy R, Ingram G, Dominy J. Darrieus turbines: the physics of self-starting. Procreedings of the Institution of Mechanical Engineers, Part A: J. Power and Energy 223(1); 2009, p 21-9

[4] Kentfield KA. The Fundamentals of Wind-driven Water pumpers. London: Taylor and Francis; 1996.

[5] Ackermann T, Soder L. Wind energy technology and current status: a review. Renewable and Sustainable Energy Reviews 4; 2000, p. 315-74.

[6] Chua KL. Design and Testing of a Vertical Axis Wind Turbine Rotor, Bachelor project, Faculty of Mechanical Engineering, University of Technology, Malaysia; 2002.

[7] Dominy R, Lunt P, Bickerdyke A, Dominy, J. Self-starting capability of a Darrieus turbine. Procreedings of the Institution of Mechanical Engineers, Part A: J. Power and Energy 221(1); 2007, p. 111-20.

[8] Worasinchai S, Ingram G, Dominy R. The physics of H-Darrieus turbine self-starting capability: flapping-wing perspective. ASME Turbo EXPO, Copenhagen, Denmark; 2012.

[9] Worasinchai, S. Small Wind Turbine Starting Behaviour, PhD thesis, School of Engineering and Computing Sciences, Durham University; 2012.

[10] Carr LW, McAlister KW, McCroskey WJ. Analysis of the Development of Dynamic Stall Based on Oscillating Airfoil Experiments, National Aeronautics and Space Administration, NASA TN D-8382; 1977.

[11] Lieshman JG. Dynamic Stall Experiments of the NACA 23012 Aerofoil, Journal of Experiments in Fluids 9; 1999, p. 49–58.

[12] Gerotakos P. An Experimental Investigation of Flow over an Oscillating Airfoil, M.Eng thesis, Department of mechanical Engineering, McGill University; 2004.

[13] Sim-Williams DB. Self-Excited Aerodynamic Unsteadiness Associated with Passenger Cars, PhD thesis, School of Engineering, University of Durham; 2001.

.